Measurements of the reduced force coefficients for H_2, N_2, CO, and CO_2 incident upon a solar panel array material, SiO_2-coated Kapton, Kapton, and Z-93-coated Al

Steven R. Cook, Mark A. Hoffbauer, David D. Clark, and Jon B. Cross
Los Alamos National Laboratory, Los Alamos, New Mexico 87545
(Received 2 October 1997; revised manuscript received 11 February 1998)

The reduced force coefficients were measured for H_2, N_2, CO, and CO_2 incident upon a solar panel array material, SiO_2-coated Kapton, Kapton, and Z-93-coated Al. The coefficients were determined by measuring both the magnitude and direction of the force exerted on the surfaces by molecular beams of the gases. Measurements were made at angles of incidence of 0°, 25°, 50°, 75°, and 85°. The forces were measured using a torsion balance with the surfaces mounted on the end of the lever arm. The absolute flux densities of the molecular beams were measured using a second torsion balance with a beam stop mounted on the lever arm that nullified the force of the scattered molecules. Flux measurements were also made using the effusive method. Standard time-of-flight techniques were used to determine the flux-weighted average velocities of the molecular beams. These velocities ranged from 1670 to 4620 m/s. The overall uncertainty in the reduced force coefficient measurements was estimated to be less than $\pm 10\%$. These measurements were used to obtain the magnitude and direction of the flux-weighted average velocity of the scattered molecules, and also the flux-weighted translational kinetic energy of the scattered molecules. Analysis of this information provided insight into the microscopic details of the gas-surface interaction potential energy surface. [S1063-651X(98)07107-4]

PACS number(s): 51.10.+y, 47.40.Ki, 34.50.Dy

I. INTRODUCTION

When a gas molecule collides with a surface, a variety of physical and chemical processes can occur. Many of these processes either result in, or are the result of, the direct exchange of energy and/or momentum between the gas and the surface. From a knowledge of the velocity and internal state distribution functions of the incident and scattered molecules, microscopic information about the gas-surface interaction and the atomic surface structure can be determined [1–3]. By directing molecular beams onto surfaces, measurements of the velocity and internal state distribution functions of the scattered molecules have provided considerable insight into understanding gas-surface interactions [4–11].

Gas-surface interactions can also be understood by studying the force exerted on a surface by an incident gas. This method of investigation is made possible because the force is directly related to the actual gas-surface interaction potential. Macroscopic average properties of the scattered molecules can also be determined from measurements of the forces exerted on surfaces by incident gases. Obtaining this information from measurements of the velocity and internal state distribution functions of the scattered molecules can be complicated by the problems associated with properly weighting these functions over speed, direction, and internal states [12,13].

Supersonic nozzle sources produce molecular beams with narrow velocity and angular distribution functions. Rotational and vibrational state selection of molecular beams can also be achieved by optical pumping schemes [14–17], and the angular momentum and spin can be oriented using electric fields and polarized light [18–22]. Using such molecular beams to make force measurements would, in principle, allow gas-surface interactions to be studied as a function of the incident energy, direction, internal state, and angular momentum orientation of the incident molecules.

The technique of examining the forces exerted on surfaces by incident gases has not been utilized as a method to understand gas-surface interactions, at least in part because a method to accurately measure these forces has not been developed. In this paper a torsion balance is discussed that was used to make measurements of the forces exerted on surfaces by molecular beams with uncertainties of about $\pm 1\%$. The force measurements were then used to determine the reduced force coefficients [23] for the various gas-surface interactions under investigation. The reduced force coefficients were then used to determine the magnitude and direction of the flux-weighted average (hereafter referred to as the average) velocity and average translational energy of the scattered molecules. Measurements were made with molecular beams of H_2, N_2, CO, and CO_2 with average velocities ranging from 1670 to 4620 m/s incident upon a solar panel array material, SiO_2-coated Kapton, Kapton, and Z-93-coated Al.

II. REDUCED FORCE COEFFICIENTS

A formalism based upon the reduced force coefficients was developed to overcome the singularity problems associated with the momentum accommodation coefficients [23,24]. The tangential f_t and normal f_n reduced force coefficients [23] are defined as

$$f_t = \frac{\overline{p}_{it} - \overline{p}_{st}}{\overline{p}_i}, \tag{1}$$

$$f_n = \frac{\overline{p}_{in} + \overline{p}_{sn}}{\overline{p}_i}, \tag{2}$$

where $\overline{p}$ is the magnitude of the average momentum, the subscripts i and s respectively refer to the incident and scat-

tered molecules, and the subscripts t and n respectively are the tangential and normal components. Using Eqs. (1) and (2), the reduced force coefficients can also be written as

$$f_t=\frac{F_t}{N_i\overline{p_i}}, \tag{3}$$

$$f_n=\frac{F_n}{N_i\overline{p_i}}, \tag{4}$$

or as

$$f_t=\sin\ \theta_i-\frac{\overline{v_s}}{\overline{v_i}}\sin\ \theta_s, \tag{5}$$

$$f_n=\cos\ \theta_i+\frac{\overline{v_s}}{\overline{v_i}}\cos\ \theta_s, \tag{6}$$

where N_i represents the number of molecules incident upon the surface per unit time, F is the magnitude of the force exerted on the surface by the molecular beam, $\overline{v}$ is the magnitude of the velocity, and θ is the angle between the average velocity and the surface normal. Equations (3) and (4) are used to determine the reduced force coefficients experimentally from measurements of F_t, F_n, N_i, and $\overline{p_i}$. Using Eqs. (5) and (6), the magnitude and direction of the average velocity of the scattered molecules can be expressed as

$$\overline{v_s}=\overline{v_i}\sqrt{(f_t-\sin\ \theta_i)^2+(f_n-\cos\ \theta_i)^2}, \tag{7}$$

$$\theta_s=\tan^{-1}\left(\frac{\sin\ \theta_i-f_t}{f_n-\cos\ \theta_i}\right). \tag{8}$$

It is assumed that the average velocity of the scattered molecules is in the plane formed by the surface normal and the average velocity of the incident molecules.

From a knowledge of the reduced force coefficients and the velocity distribution function of the incident molecules, the average translational energy of the scattered molecules can be accurately approximated for many applications. The approximation method makes use of two types of energy accommodation coefficients. The definition of the first coefficient ϵ is based upon the average translational kinetic energies of the incident and scattered molecules, and is given by

$$\epsilon=\frac{\overline{e_{ik}}-\overline{e_{sk}}}{\overline{e_{ik}}-\overline{e_{dk}}}=\frac{\overline{v_i^2}-\overline{v_s^2}}{\overline{v_i^2}-4kT/m}, \tag{9}$$

where the subscript k represents the kinetic energy associated with translation, the subscript d represents diffuse scattering with complete thermal accommodation, m is the mass of individual gas molecules, k is Boltzmann's constant, T is the temperature of the scattering surface, and $\overline{v^2}$ is the average of the velocity squared. The quantity $4kT/m$ is the average of the velocity squared of the scattered molecules assuming diffuse scattering from the surface with complete thermal accommodation. The second coefficient ϵ' is defined using the average velocity of the incident and scattered molecules, and is given by

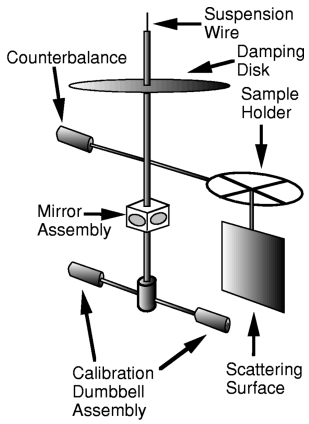

FIG. 1. Schematic diagram of the torsion balance used to measure the normal and tangential force components.

$$\epsilon'=\frac{\overline{v_i^2}-\overline{v_s^2}}{\overline{v_i^2}-\pi kT/2m}. \tag{10}$$

Note that both ϵ and ϵ' range between zero for pure specular reflection and one for diffuse scattering with complete thermal accommodation. With the approximation that ϵ and ϵ' are equal,

$$\overline{v_s^2}=\overline{v_i^2}-\epsilon'(\overline{v_i^2}-4kT/m). \tag{11}$$

With a knowledge of the reduced force coefficients and the velocity distribution function of the incident molecules, $\overline{v_i^2}$, $\overline{v_i^2}$, and ϵ' can be determined. Once these quantities are known, Eq. (11) can be used to determine $\overline{v_s^2}$. The uncertainty associated with the approximation of equating ϵ with ϵ' has been shown to be less than $\pm 1\%$ for gas-surface interactions where the average energy of the incident molecules is large compared to kT [25].

III. EXPERIMENTAL DETAILS

The gas-surface interactions investigated were those between the plume gases emitted by the reaction control jets on the Space Shuttle, and the materials to be used in the construction of the large solar array panels on the International Space Station. Understanding the complicated gas-surface interactions is needed to make accurate predictions of the forces exerted on the solar array panels by the plumes before a final design of the panels can be made.

Measurements were made using the solar panel array material to be utilized on the International Space Station, a polyimide plastic with the trade name Kapton, SiO_2-coated Kapton, and aluminum coated with a material used for thermal insulation on spacecraft surfaces called Z-93. The solar panel is also SiO_2 coated. The primary gas components emitted by the reaction control jets on the Space Shuttle are H_2O, H_2, N_2, CO, and CO_2, all of which result from the reaction of monomethyl hydrazine ($CH_3N_2H_4$) and nitrogen tetroxide (N_2O_4). Measurements were made with each of these gases,

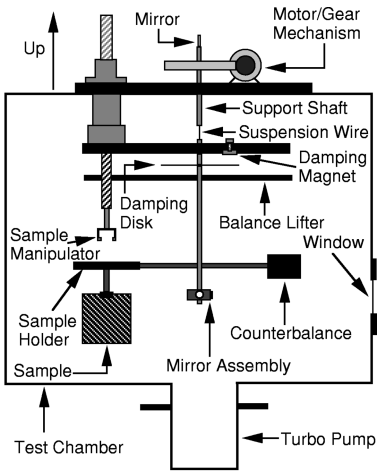

FIG. 2. Schematic diagram of the torsion balance manipulator. The molecular beam propagation direction is into the page.

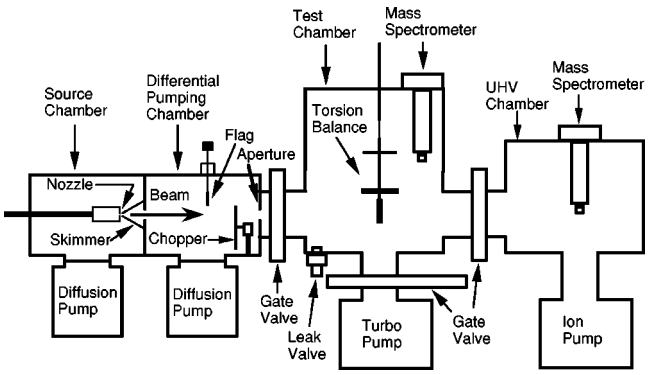

FIG. 4. Schematic diagram of the apparatus used to make the momentum transfer measurements. The molecular beam produced by the nozzle passes through a skimmer into the differential pumping chamber, then through an aperture before entering the test chamber. The mass spectrometer and torsion balance are housed in the test chamber.

except H_2O, incident upon all four surfaces. All measurements were made with each surface at room temperature, and no effort was made to specially prepare or clean the surfaces in any way.

A. The torsion balance

Figure 1 shows a simplified drawing of the specialized torsion balance used to measure the forces exerted on the scattering surfaces by the molecular beams. The torsion balance was constructed from copper. This material has a small magnetic susceptibility, excellent electrical conductivity, and good vacuum characteristics. Thus errors due to stray magnetic fields, charge buildup, and outgassing on the surface of the balance were eliminated. Notches cut into the sample holder allowed the angle of incidence of the molecular beam to be adjusted in 5° increments under vacuum from 0° to 85°. Measurements were made at angles of incidence of 0°, 25°, 50°, 75°, and 85°. The sample holder was adjusted using the mechanism shown schematically in Fig. 2. To adjust the angular position of the sample, tension was taken off of the suspension wire by lifting the balance with the balance lifting mechanism shown in Fig. 2. The mechanism securely held the balance by the damping disk, eliminating the possibility of breaking the wire with the sample manipulator during adjustment. To keep the moment of inertia of the torsion balance to a minimum, the sample holder was constructed from Al. The crossbeam and central axis of the torsion balance were constructed from 3.18-mm-diameter cylindrical rod. The central axis length was 30 cm, and the torsion balance lever arm length, defined to be the distance from the axis of rotation to the center of the beam stop, was 6.03 cm. The damping disk was circular with a diameter of 7.5 cm, and was constructed from 0.38-mm-thick shim stock. The overall mass of the torsion balance was approximately 82 g. A gold coated tungsten suspension wire was used that had a diameter of 25 μm and a length of approximately 10 cm.

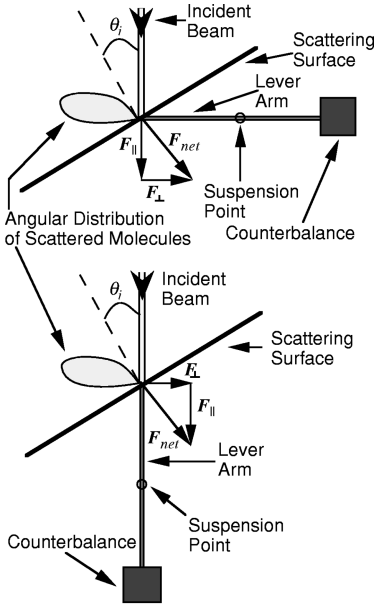

FIG. 3. Schematic diagram of the torsion balance configurations used to measure the force components perpendicular and parallel to the molecular beam. The top configuration is used to measure the force component parallel to the beam, while the bottom configuration is used to measure the component perpendicular to the beam. The view is looking down on the torsion balance assembly from above.

Measurements were made with the torsion balance lever arm in two configurations to determine both the magnitude and direction of the force exerted on the sample by the molecular beam. The force component parallel to the molecular beam $F_{\parallel}$ was measured with the lever perpendicular to the beam, while the force component perpendicular to the beam $F_{\perp}$ was measured with the lever arm parallel to the beam, as shown in Fig. 3. During both measurements, the angle of incidence the beam made with respect to the scattering surface was the same. Once both components were measured, the normal and tangential components were calculated using

$$F_t = F_{\parallel} \sin \theta_i - F_{\perp} \cos \theta_i \tag{12}$$

and

$$F_n = F_{\parallel} \cos \theta_i + F_{\perp} \sin \theta_i . \tag{13}$$

TABLE I. Comparison of the molecular beam flux measurements made using the effusive method with those made using the torsion balance.

Gas mixture	Nozzle temp. (K)	Nozzle press. (kPa)	$\overline{v_i}$ H_2 (m/s)	$\overline{v_i}$ Seed gas (m/s)	Φ H_2 eff. (mol/s cm^2)	Φ Seed gas eff. (mol/s cm^2)	Φ Seed tor. bal. (mol/s cm^2)	% diff.	Seed gas flux %
5%N_2,95%H_2	295	20	2060	1870	2.37×10^{16}	7.96×10^{15}	7.58×10^{15}	4.9	25
5%CO,95%H_2	295	20	2080	1870	2.24×10^{16}	7.73×10^{15}	7.59×10^{15}	1.8	26
5%CO_2,95%H_2	295	20	1890	1670	1.52×10^{16}	7.36×10^{15}	7.22×10^{15}	1.9	33
5%N_2,95%H_2	775	67	3780	3180	4.81×10^{16}	1.74×10^{16}	1.73×10^{16}	0.6	27
5%CO,95%H_2	775	67	3800	3190	4.59×10^{16}	1.74×10^{16}	1.69×10^{16}	2.9	27
5%CO_2,95%H_2	775	67	3490	2840	3.00×10^{16}	1.47×10^{16}	1.61×10^{16}	9.1	33
100%H_2	295	20	2590	N.A.	5.79×10^{16}	N.A.	5.78×10^{16}	0.2	N.A.
100%H_2	775	67	4620	N.A.	1.23×10^{17}	N.A.	1.25×10^{17}	1.6	N.A.

Detailed descriptions of how this torsion balance was used to measure the forces, and how the suspension wire was calibrated, are given elsewhere for a nearly identical torsion balance that was used to measure the absolute flux densities of the molecular beams [26].

B. Molecular beam source and characterization

Figure 4 shows a schematic diagram of the apparatus used to make the momentum transfer measurements. The supersonic nozzle source produces molecular beams with large flux densities and narrow velocity and angular distributions. A source nearly identical to the one utilized in this experiment was described in detail elsewhere [27]. The nozzle was constructed from Ni with an orifice diameter of 130 μm, and was resistively heated by passing currents up to 900 A through the nozzle tip at rms voltages between 3 and 7 V. Heat generated by the source during operation was dissipated by flowing water through the nozzle mounting block and copper tubing soldered onto the inner walls of the housing chamber. The entrance aperture to the test chamber had an

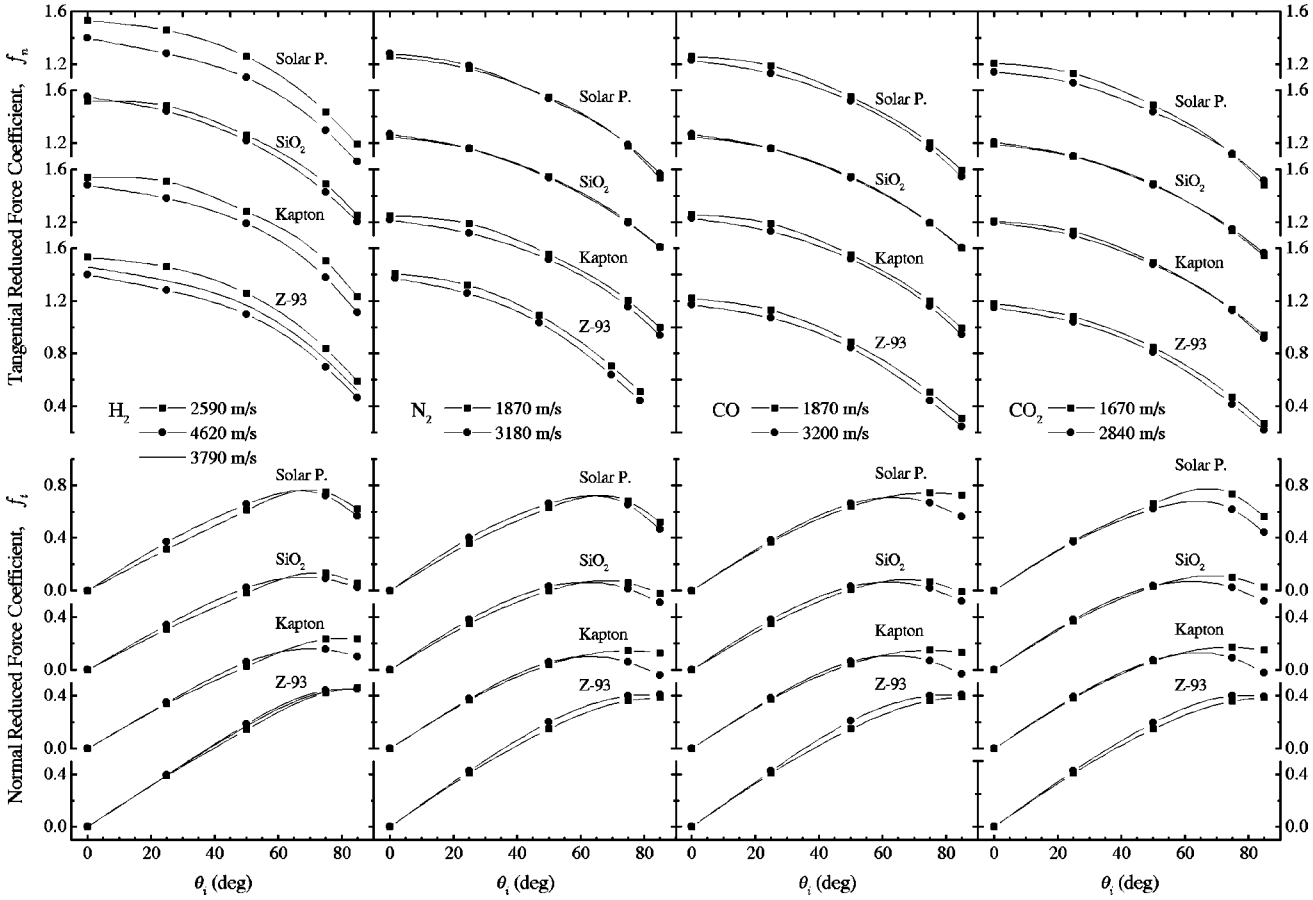

FIG. 5. The normal and tangential reduced force coefficients for H_2, N_2, CO, and CO_2 incident upon the solar panel array material, SiO_2-coated Kapton, Kapton, and Z-93-coated Al at the indicated average incident velocities. The values of the reduced force coefficients for each plot are determined from the vertical scale immediately to the left of the points at θ_i equal to zero.

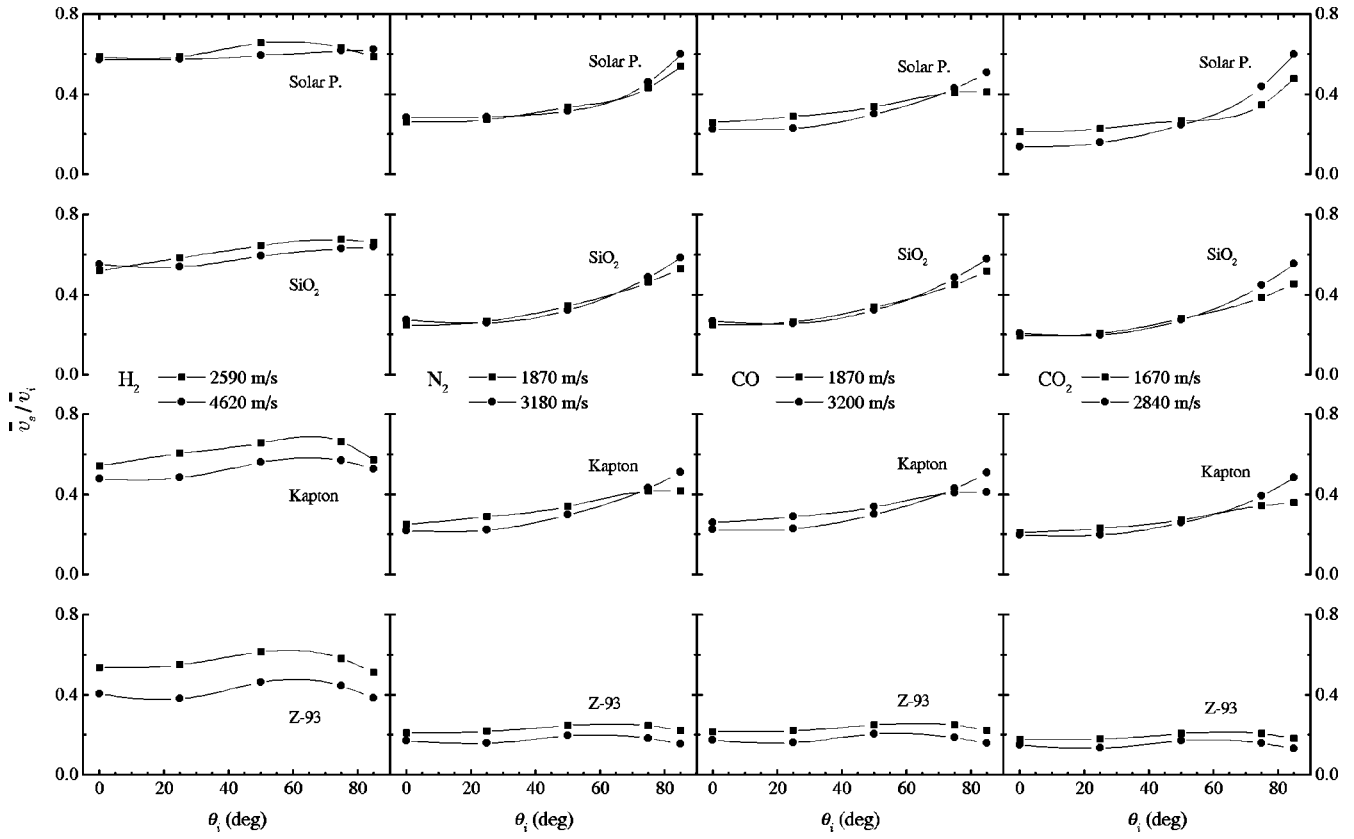

FIG. 6. The ratio $\overline{v_s}/\overline{v_i}$ for H_2, N_2, CO, and CO_2 incident upon the solar panel array material, SiO_2-coated Kapton, Kapton, and Z-93-coated Al at the indicated average incident velocities.

area of 6.47 mm^2, and was located 16.4 cm from the nozzle and 19.9 cm in front of the scattering surface mounted on the torsion balance.

The seeded beam method [28] was used to produce high energy beams of N_2, CO, and CO_2. The basic concept of this method is to flow a gas mixture through the nozzle orifice containing a small percentage of heavy molecules and a large percentage of light molecules. During the supersonic expansion process, the heavy molecules collide predominantly with the light molecules and attain nearly the same beam velocity. The light molecules in the mixture are referred to as the carrier gas, while the heavy molecules are referred to as the seed gas. Measurements were made with mixtures containing 5% of the seed gases using H_2 as the carrier gas. The source was operated at stagnation pressures behind the nozzle of 20 kPa with the nozzle at room temperature, and at 67 kPa with the nozzle at 775 K.

The average velocities of the molecular beams were calculated from the measured velocity distribution functions of the beams. The distribution functions were measured using standard time-of-flight techniques [29]. A complete description of the time-of-flight apparatus, and how it was used to determine the velocity distribution functions of the molecular beams, is given elsewhere [25,26].

Absolute flux measurements of the molecular beams were made using both the effusive method and a torsion balance fitted with a beam stop that eliminated the torque due to the exiting gas molecules. Complete descriptions of these systems, how they were used to make the absolute flux density measurements, and a comparison of the results obtained using the two methods is given elsewhere [26].

C. Error analysis

From Eqs. (3) and (4), the total error in the reduced force coefficient measurements is given by

$$\frac{\Delta f_t}{f_t}=\frac{\Delta F_t}{F_t}+\frac{\Delta\Phi}{\Phi}+\frac{\Delta A}{A}+\frac{\Delta\overline{v_i}}{\overline{v_i}} \tag{14}$$

and

$$\frac{\Delta f_n}{f_n}=\frac{\Delta F_n}{F_n}+\frac{\Delta\Phi}{\Phi}+\frac{\Delta A}{A}+\frac{\Delta\overline{v_i}}{\overline{v_i}}, \tag{15}$$

where

$$N_i=A\Phi, \tag{16}$$

A is the area of the entrance aperture to the torsion balance chamber, and Φ is the absolute flux density of the molecular beam. The uncertainties in these quantities have been thoroughly dealt with elsewhere [26]. Uncertainties in the force measurements were shown to be less than or equal to $\pm 1.3\%$. The uncertainties in the flux measurements by both methods were less than or equal to $\pm 5\%$. The aperture area uncertainty was $\pm 1.7\%$, and the uncertainties in the average velocities of the molecular beams were approximately $\pm 2\%$. Therefore, the overall uncertainty in the reduced force coefficient measurements was about $\pm 10\%$.

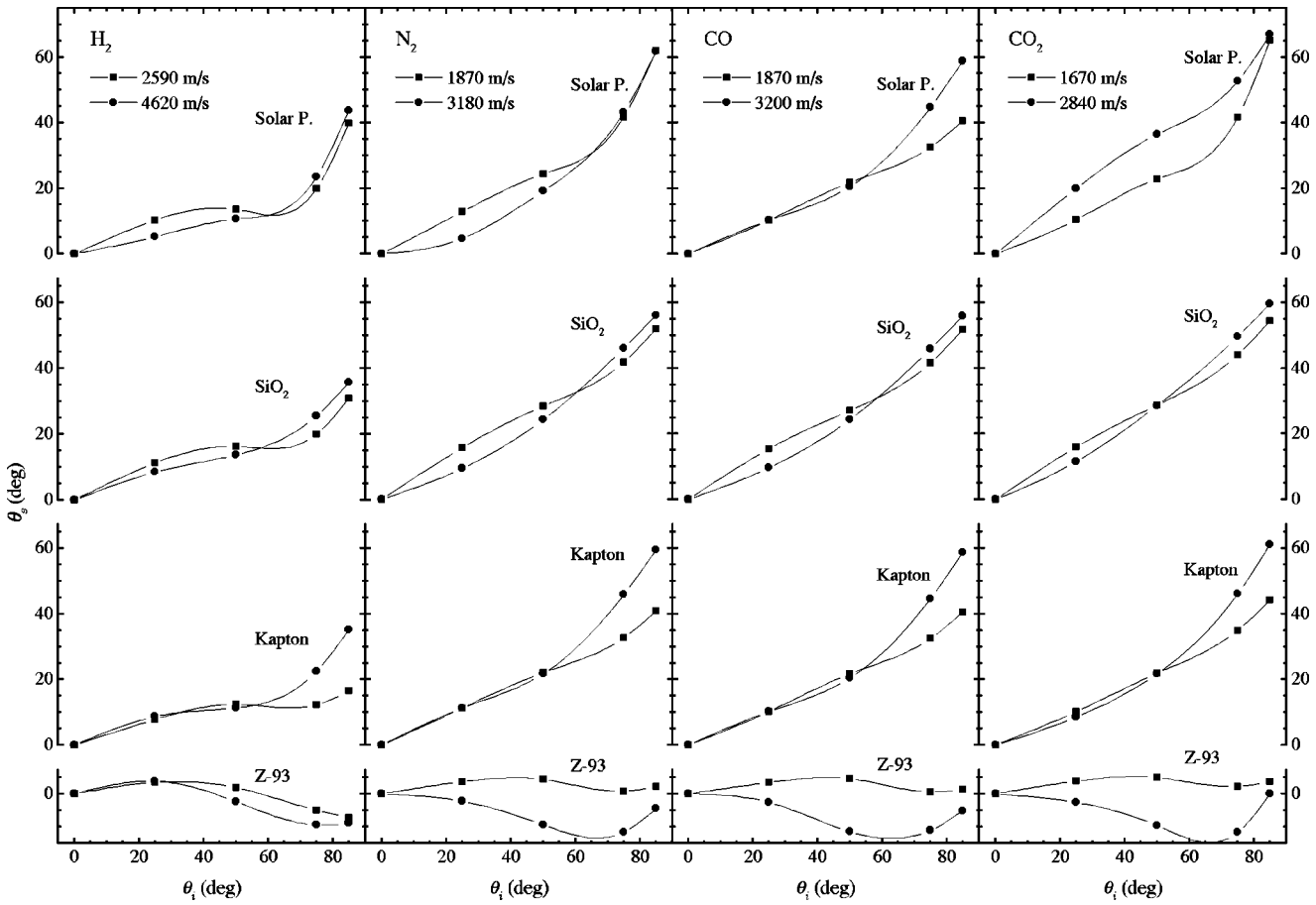

FIG. 7. The scattering angle θ_s for H_2, N_2, CO, and CO_2 incident upon the solar panel array material, SiO_2-coated Kapton, Kapton, and Z-93-coated Al at the indicated average incident velocities.

IV. EXPERIMENTAL RESULTS AND DISCUSSION

A. Time-of-flight and molecular beam flux density measurements

Details concerning the production of the molecular beams, as well as their average velocities and flux densities are summarized in Table I. The gas mixtures, nozzle temperatures, and nozzle pressures are listed, as well as the measured average velocities of the molecular beam components. The final two columns give the percent difference between the flux density measurements made using the two methods and the experimentally determined percentage of the seed gas in the molecular beams.

Forces exerted on the beam stop by the beams ranged from 3.24×10^{-8} N, for the pure H_2 beam with the nozzle at room temperature, to 2.39×10^{-7} N for he beam produced by the 5% CO_2 mixture with the nozzle at 775 K. The results show that the percent differences between the torsion balance and effusive methods for all the molecular beams were less than 10%. The two methods are based on entirely different physical processes, yet they yield results that are in exceptional agreement for a wide variety of molecular beams. Therefore, any appreciable unknown systematic errors are unlikely, and accurate flux measurements could be made using either method. Because the torsion balance method requires the average velocity of the molecular beam, these results also imply that the time-of-flight method yields accurate results.

Table I shows that with the source at a stagnation pressure of 20 kPa, N_2 and CO were approximately 25% of the total molecular beam flux, while CO_2 was approximately 33%. When the nozzle was heated to 775 K and the pressure increased to 67 kPa, these percentages remained essentially unchanged. For a molecular beam produced using a binary stagnation gas mixture with a small seed gas percentage, these results imply that the seed gas percentage of the total molecular beam flux is nearly independent of both the stagnation pressure and nozzle temperature.

In the discussion of molecular beams composed of binary mixtures by Miller [30], the perpendicular speed ratio is defined as

$$\frac{\overline{v}}{\sqrt{2kT_{\perp}/m}}, \tag{17}$$

which represents the ratio of the translational velocity of the beam to the velocity perpendicular to the beam. The perpendicular temperature $T_{\perp}$ and velocity $\overline{v}$ of the seed gas are nearly the same as $T_{\perp}$ and $\overline{v}$ of the carrier gas. Thus the heavier mass component will have the smallest perpendicular velocity component and the largest perpendicular speed ratio. With a smaller perpendicular velocity component, the heavier gas stays focused along the beam center line, while the lighter gas has a larger angular divergence. This focusing effect explains why the seed gas flux percentages were

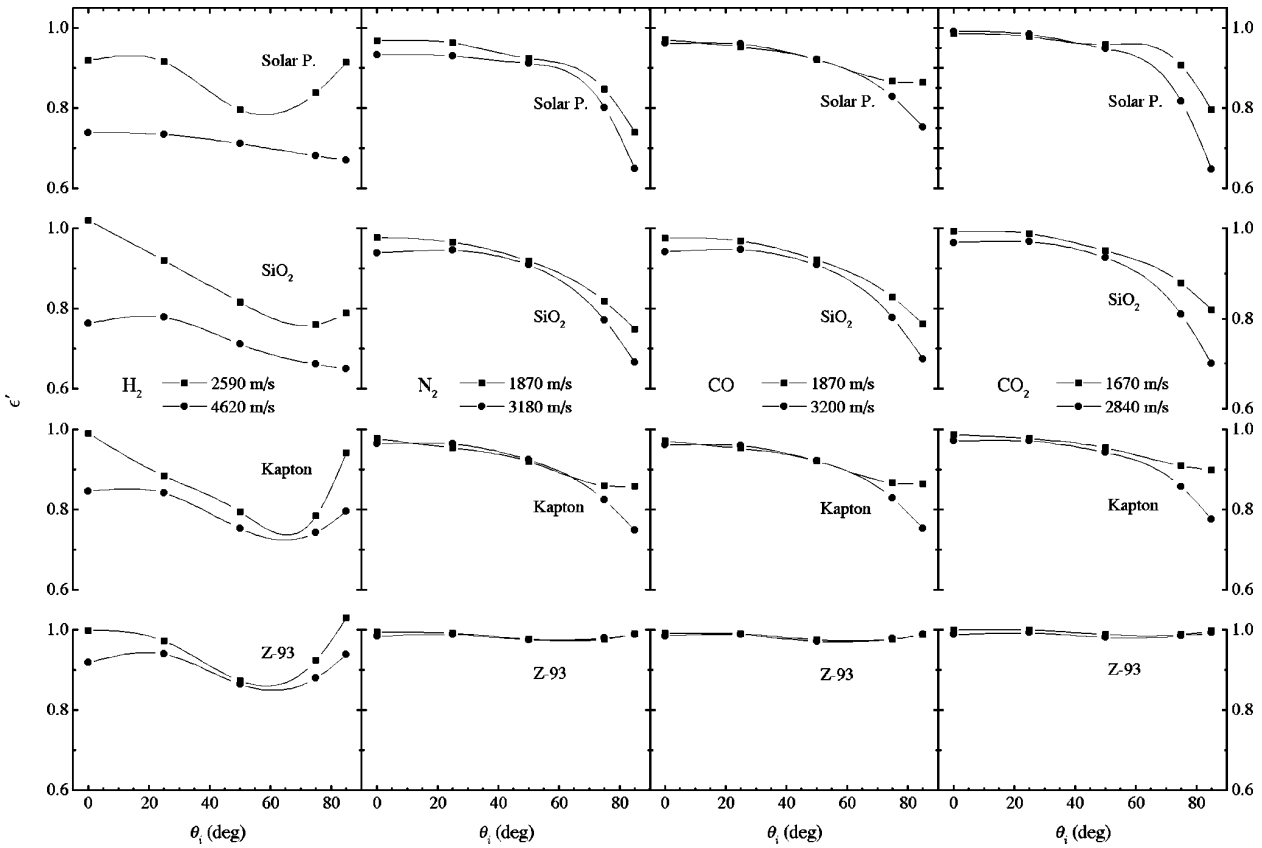

FIG. 8. The energy accommodation coefficient ϵ' for H_2, N_2, CO, and CO_2 incident upon the solar panel array material, SiO_2-coated Kapton, Kapton, and Z-93-coated Al at the indicated average incident velocities.

TABLE II. Experimental results for H_2 scattered from the indicated surfaces.

θ_i (deg)	f_t	f_n	$\overline{v_s}$ (m/s)	θ_s (deg)	ϵ'	$\overline{v_s^2}$ $(m/s)^2$	f_t	f_n	$\overline{v_s}$ (m/s)	θ_s (deg)	ϵ'	$\overline{v_s^2}$ $(m/s)^2$
Solar panel	$\overline{v_i}=2590$ (m/s)						$\overline{v_i}=4620$ (m/s)					
0	0	1.59	1520	0	0.918	5.02×10^6	0	1.57	2650	0	0.738	9.32×10^6
25	0.317	1.48	1520	10.3	0.916	5.02×10^6	0.370	1.48	2660	5.25	0.735	9.36×10^6
50	0.612	1.28	1700	13.6	0.796	5.25×10^6	0.656	1.23	2740	10.7	0.712	9.77×10^6
75	0.750	0.854	1640	19.9	0.839	5.17×10^6	0.720	0.823	2850	23.5	0.682	1.03×10^7
85	0.619	0.539	1520	39.8	0.915	5.03×10^6	0.564	0.538	2800	43.8	0.670	1.05×10^7
SiO_2/Kapton												
0	0	1.52	1350	0	1.02	4.82×10^6	0	1.55	2550	0	0.763	8.90×10^6
25	0.307	1.48	1510	11.4	0.920	5.02×10^6	0.343	1.44	2490	8.54	0.779	8.62×10^6
50	0.584	1.26	1670	16.4	0.816	5.22×10^6	0.624	1.22	2750	13.8	0.711	9.79×10^6
75	0.733	0.893	1750	20.1	0.760	5.32×10^6	0.693	0.828	2920	26.6	0.661	1.06×10^7
85	0.656	0.653	1710	31.0	0.789	5.27×10^6	0.624	0.606	2950	35.7	0.650	1.08×10^7
Kapton												
0	0	1.54	1400	0	0.990	4.88×10^6	0	1.48	2210	0	0.846	7.48×10^6
25	0.340	1.51	1570	7.80	0.885	5.08×10^6	0.349	1.38	2240	8.81	0.841	7.56×10^6
50	0.625	1.28	1700	12.4	0.794	5.26×10^6	0.655	1.19	2590	11.4	0.753	9.06×10^6
75	0.826	0.907	1720	12.2	0.784	5.28×10^6	0.748	0.784	2630	22.5	0.743	9.24×10^6
85	0.833	0.635	1480	16.6	0.942	4.97×10^6	0.694	0.517	2430	35.1	0.796	8.34×10^6
Z-93/Al												
0	0	1.53	1380	0	0.999	4.87×10^6	0	1.40	1870	0	0.919	6.24×10^6
25	0.388	1.46	1430	3.59	0.973	4.91×10^6	0.396	1.28	1750	3.99	0.940	5.88×10^6
50	0.745	1.26	1590	1.96	0.873	5.11×10^6	0.785	1.10	2130	−2.31	0.865	7.17×10^6
75	1.02	0.839	1510	−5.02	0.925	5.01×10^6	1.04	0.698	2060	−9.41	0.880	6.90×10^6
85	1.06	0.594	1320	−7.25	1.03	4.80×10^6	1.05	0.465	1770	−8.85	0.938	5.92×10^6

TABLE III. Experimental results for N_2 scattered from the indicated surfaces.

θ_i (deg)	f_t	f_n	$\overline{v_s}$ (m/s)	θ_s (deg)	ϵ'	$\overline{v_s^2}$ (m/s)^2	f_t	f_n	$\overline{v_s}$ (m/s)	θ_s (deg)	ϵ'	$\overline{v_s^2}$ (m/s)^2
Solar panel	$\overline{v_i}=1870$(m/s)						$\overline{v_i}=3180$(m/s)					
0	0	1.26	491	0	0.969	4.48×10^5	0	1.28	896	0	0.933	1.05×10^6
25	0.362	1.17	513	12.8	0.963	4.69×10^5	0.400	1.19	912	4.60	0.930	1.05×10^6
50	0.628	0.949	629	24.3	0.924	5.94×10^5	0.662	0.942	1010	19.1	0.912	1.24×10^5
75	0.679	0.581	808	41.7	0.847	8.37×10^5	0.653	0.593	1460	43.1	0.801	2.35×10^6
85	0.522	0.340	1010	61.9	0.740	1.18×10^6	0.468	0.371	1910	61.8	0.649	3.88×10^6
SiO_2/Kapton												
0	0	1.25	464	0	0.977	4.23×10^5	0	1.27	869	0	0.938	9.72×10^5
25	0.350	1.16	501	15.8	0.966	4.57×10^5	0.380	1.16	820	9.52	0.946	8.89×10^5
50	0.602	0.945	645	28.5	0.918	6.13×10^5	0.633	0.937	1030	24.3	0.908	1.28×10^6
75	0.658	0.603	865	41.9	0.819	9.29×10^5	0.613	0.597	1550	46.2	0.772	2.65×10^6
85	0.578	0.412	993	52.1	0.748	1.15×10^6	0.509	0.412	1860	56.2	0.666	3.71×10^6
Kapton												
0	0	1.25	465	0	0.977	4.25×10^5	0	1.22	698	0	0.965	7.02×10^5
25	0.366	1.19	540	11.3	0.954	4.96×10^5	0.379	1.12	704	11.4	0.964	7.11×10^5
50	0.638	0.959	639	22.1	0.920	6.07×10^5	0.656	0.918	943	21.8	0.925	1.11×10^6
75	0.740	0.609	781	32.8	0.860	7.98×10^5	0.656	0.559	1370	45.9	0.825	2.11×10^6
85	0.722	0.403	784	40.9	0.858	8.02×10^5	0.555	0.347	1630	59.5	0.748	2.88×10^6
Z-93/Al												
0	0	1.21	395	0	0.994	3.68×10^5	0	1.17	539	0	0.985	5.05×10^5
25	0.408	1.12	409	3.82	0.991	3.78×10^5	0.429	1.06	499	−2.20	0.989	4.62×10^5
50	0.747	0.889	463	4.45	0.977	4.23×10^5	0.798	0.834	617	−9.33	0.976	5.96×10^5
75	0.962	0.506	465	0.857	0.977	4.23×10^5	1.00	0.438	583	−11.6	0.980	5.54×10^5
85	0.987	0.308	414	2.34	0.990	3.82×10^5	1.01	0.241	492	−4.48	0.989	4.56×10^5

TABLE IV. Experimental results for CO scattered from the indicated surfaces.

θ_i (deg)	f_t	f_n	$\overline{v_s}$ (m/s)	θ_s (deg)	ϵ'	$\overline{v_s^2}$ (m/s)^2	f_t	f_n	$\overline{v_s}$ (m/s)	θ_s (deg)	ϵ'	$\overline{v_s^2}$ (m/s)^2
Solar panel	$\overline{v_i}=1870$(m/s)						$\overline{v_i}=3200$(m/s)					
0	0	1.26	488	0	0.970	4.46×10^5	0	1.29	913	0	0.931	1.05×10^6
25	0.366	1.18	524	11.7	0.959	4.80×10^5	0.403	1.19	926	3.90	0.929	1.07×10^6
50	0.634	0.948	624	23.4	0.925	5.89×10^5	0.665	0.945	1020	18.5	0.911	1.26×10^6
75	0.688	0.577	793	41.2	0.855	8.15×10^5	0.661	0.590	1440	42.6	0.808	2.30×10^6
85	0.530	0.338	993	61.7	0.749	1.15×10^6	0.472	0.365	1900	62.1	0.656	3.85×10^6
SiO_2/Kapton												
0	0	1.25	467	0	0.976	4.26×10^5	0	1.27	857	0	0.941	9.52×10^5
25	0.352	1.16	497	15.4	0.968	4.54×10^5	0.380	1.16	819	9.65	0.947	8.87×10^5
50	0.611	0.944	635	27.2	0.921	6.02×10^5	0.634	0.935	1030	24.3	0.909	1.27×10^6
75	0.666	0.596	845	41.7	0.829	8.96×10^5	0.619	0.595	1550	45.9	0.777	2.62×10^6
85	0.589	0.406	970	51.9	0.762	1.11×10^6	0.518	0.411	1850	56.0	0.675	3.66×10^6
Kapton												
0	0	1.26	486	0	0.971	4.44×10^5	0	1.23	725	0	0.962	7.40×10^5
25	0.371	1.19	544	10.3	0.953	5.00×10^5	0.382	1.13	734	10.2	0.960	7.53×10^5
50	0.641	0.956	633	21.7	0.922	5.99×10^5	0.661	0.925	965	20.4	0.921	1.15×10^6
75	0.745	0.603	766	32.6	0.867	7.76×10^5	0.665	0.563	1370	44.7	0.828	2.10×10^6
85	0.728	0.400	772	40.6	0.864	7.84×10^5	0.562	0.350	1620	58.8	0.753	2.87×10^6
Z-93/Al												
0	0	1.22	404	0	0.992	3.74×10^5	0	1.17	550	0	0.984	5.16×10^5
25	0.409	1.13	414	3.52	0.990	3.83×10^5	0.429	1.07	511	−2.46	0.988	4.74×10^5
50	0.746	0.890	466	4.65	0.976	4.25×10^5	0.807	0.844	658	−11.4	0.971	6.47×10^5
75	0.963	0.507	465	0.687	0.977	4.24×10^5	1.00	0.440	592	−11.1	0.979	5.65×10^5
85	0.991	0.309	416	1.45	0.989	3.84×10^5	1.01	0.244	503	−5.19	0.989	4.66×10^5

TABLE V. Experimental results for CO_2 scattered from the indicated surfaces.

θ_i (deg)	f_t	f_n	$\overline{v_s}$ (m/s)	θ_s (deg)	ϵ'	$\overline{v_s^2}$ (m/s)^2	f_t	f_n	$\overline{v_s}$ (m/s)	θ_s (deg)	ϵ'	$\overline{v_s^2}$ (m/s)^2
Solar panel	$\overline{v_i}=1670$(m/s)						$\overline{v_i}=2840$(m/s)					
0	0	1.21	355	0	0.986	2.60×10^5	0	1.14	387	0	0.992	2.86×10^5
25	0.381	1.13	379	10.5	0.979	2.77×10^5	0.369	1.06	451	19.9	0.985	3.40×10^5
50	0.661	0.891	449	22.9	0.958	3.33×10^5	0.619	0.841	700	36.5	0.949	6.30×10^5
75	0.734	0.519	582	41.7	0.907	4.64×10^5	0.618	0.525	1240	52.6	0.817	1.70×10^6
85	0.562	0.288	799	65.2	0.769	7.52×10^5	0.444	0.322	1700	67.0	0.647	3.07×10^5
SiO_2/Kapton												
0	0	1.19	324	0	0.994	2.39×10^5	0	1.21	587	0	0.968	4.83×10^5
25	0.366	1.10	344	16.0	0.988	2.53×10^5	0.383	1.10	564	11.6	0.971	4.56×10^5
50	0.630	0.889	469	28.9	0.951	3.50×10^5	0.635	0.883	777	28.6	0.935	7.45×10^5
75	0.699	0.536	642	44.0	0.880	5.35×10^5	0.625	0.548	1270	49.6	0.809	1.76×10^6
85	0.627	0.350	757	54.5	0.820	6.89×10^5	0.518	0.368	1580	59.6	0.700	2.64×10^6
Kapton												
0	0	1.21	351	0	0.987	2.57×10^5	0	1.20	561	0	0.972	4.52×10^5
25	0.381	1.13	388	10.3	0.977	2.83×10^5	0.393	1.10	559	8.55	0.972	4.50×10^5
50	0.664	0.897	457	21.9	0.955	3.39×10^5	0.670	0.883	735	21.7	0.943	6.80×10^5
75	0.769	0.541	574	35.0	0.910	4.56×10^5	0.685	0.530	1110	46.1	0.857	1.38×10^6
85	0.745	0.345	601	44.2	0.899	4.86×10^5	0.574	0.321	1370	61.1	0.776	2.03×10^6
Z-93/Al												
0	0	1.18	295	0	1.00	2.22×10^5	0	1.15	421	0	0.989	3.13×10^5
25	0.410	1.08	297	3.93	1.00	2.23×10^5	0.429	1.04	380	−2.52	0.993	2.80×10^5
50	0.748	0.848	345	5.07	0.988	2.53×10^5	0.794	0.809	479	−9.54	0.982	3.66×10^5
75	0.957	0.467	348	2.34	0.988	2.55×10^5	0.998	0.414	449	−11.6	0.986	3.38×10^5
85	0.984	0.270	307	3.85	0.998	2.29×10^5	0.996	0.219	373	0.076	0.993	2.75×10^5

higher than the percentages of the seed gases contained in the stagnation mixtures, and why the CO_2 flux percentages were higher than the N_2 and CO percentages.

B. Momentum transfer measurements

1. The interpolation method

For molecular beams composed of binary gas mixtures, the torsion balance measures the total force exerted on the scattering surface and does not distinguish between the forces exerted by the seed and carrier gases. To determine the reduced force coefficients for binary gas mixtures, it is necessary to obtain from the torsion balance measurements the force due to each beam species. An interpolation method was used to calculate the force exerted on the samples by the carrier gas from measurements of the reduced force coefficients for pure beams of the carrier gas at two average velocities. The force due to the seed gas was obtained by subtracting the force due to the carrier gas from the total force measured using the torsion balance.

Equations. (5) and (6) show that the reduced force coefficients are independent of the flux of the incident molecular beam and are, therefore, ideally suited for studying $\overline{v_s}$ as a function of $\overline{v_i}$. The measured reduced force coefficients for the carrier gas H_2 at the two beam velocities incident upon all four surfaces are shown as a function of the angle of incidence in the left column of Fig. 5. The data indicate that the coefficients have a weak dependence upon the average velocity of the incident molecular beams. Thus, for a particular angle of incidence, $\overline{v_s}$ is nearly proportional to $\overline{v_i}$. This result implies that only small errors will be introduced by assuming that unknown values of f_t and f_n can be obtained by linearly interpolating between the measured values. Using Z-93-coated Al as an example, the two measured values of f_n at 25° were

$$f_n(2590\ \text{m/s},\ 25°)=1.46,$$

$$f_n(4620\ \text{m/s},\ 25°)=1.28. \tag{18}$$

When 5% N_2 was seeded in H_2, with the nozzle at 775 K, the average velocity of H_2 in the beam was 3790 m/s. Assuming that f_n(3790 m/s, 25°) can be obtained by linearly interpolating between the two values given in Eq. (18),

$$f_n(3790\ \text{m/s},\ 25°)=1.35. \tag{19}$$

The other values of f_t and f_n for 3790 m/s H_2 are shown as solid lines without symbols in Fig. 5 for Z-93-coated Al. This method was then repeated for all the molecular beams incident upon all four surfaces. Once the values of f_t and f_n were known, Eqs. (3) and (4) were used to calculate the portion of the total force components due to H_2. The force components due to H_2 were then subtracted from the total force components measured using the torsion balance to obtain the components due to each specific seed gas.

2. Discussion

Figures 5–8 and Tables II–V show the experimental results for the gases incident upon the surfaces with the indi-

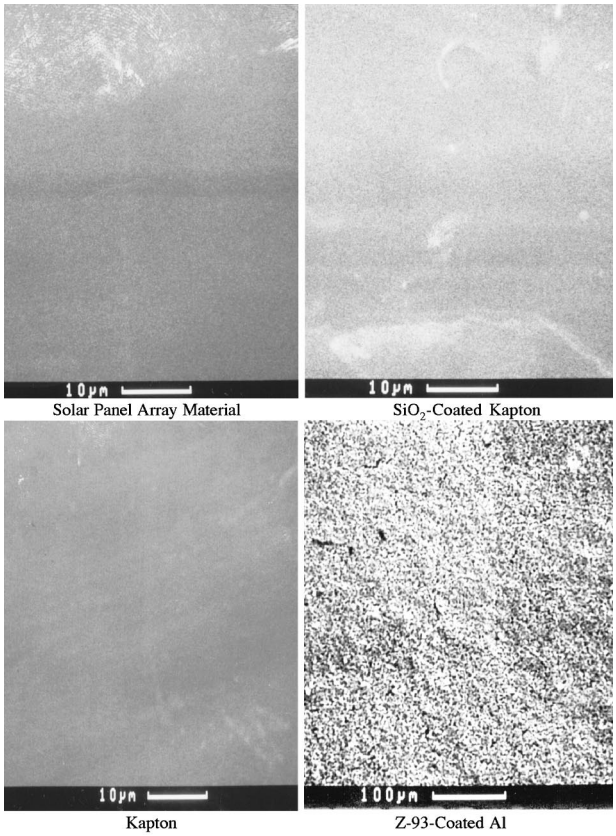

FIG. 9. Scanning electron microscope images of the four scattering surfaces used in these experiments.

cated average velocities. For a particular gas, the results for the solar panel array material, SiO_2-coated Kapton, and Kapton have many similarities, while the results for Z-93-coated Al are unique. In general, the results for Z-93-coated Al appear to be adequately explained by diffuse scattering with near complete thermal accommodation. Scanning electron microscope images of the four surfaces, shown in Fig. 9, revealed that Z-93-coated Al was rough on a scale greater than 100 μm, while the other three surfaces were smooth on a scale less than 10 μm. This dramatic difference in surface roughness would account for the differences in the scattering behavior for Z-93-coated Al, and explains why scattering from this surface was almost diffuse with near complete thermal accommodation.

For the solar panel array material, SiO_2-coated Kapton, and Kapton, some general descriptions of the scattering behavior can be made. Figures 6 and 7 show that as the angle of incidence increases, both $\overline{v_s}/\overline{v_i}$ and θ_s generally increase. At angles of incidence less than or equal to 50°, $\overline{v_s}/\overline{v_i}$ and θ_s are generally larger for the beam with the smaller average incident velocity. At angles of incidence greater than or equal to 75°, $\overline{v_s}/\overline{v_i}$ and θ_s are generally larger for the beam with the larger average incident velocity. The molecular beams of H_2 are the exception, however, where $\overline{v_s}/\overline{v_i}$ actually decreases at large angles of incidence for some cases.

To account for these results, simple models show that the energy transfered to surface molecules by incident gases decreases as the angle of incident increases [31]. This fact would explain why the average velocity of the scattered molecules increases as the angle of incidence increases. Since the normal momentum component of the incident molecules decreases as the angle of incidence increases, the depth of penetration made by the incident molecules into the repulsive potential energy barrier associated with the surface molecules would be expected to decrease as the angle of incidence increases. Thus the interaction with the strong repulsive potential barrier at the surface would be weaker for large angles of incidence, and the direction of the force exerted on the gas molecules would be nearer to the surface normal. The result would be more specular scattering with an increase in $\overline{v_s}/\overline{v_i}$ and θ_s.

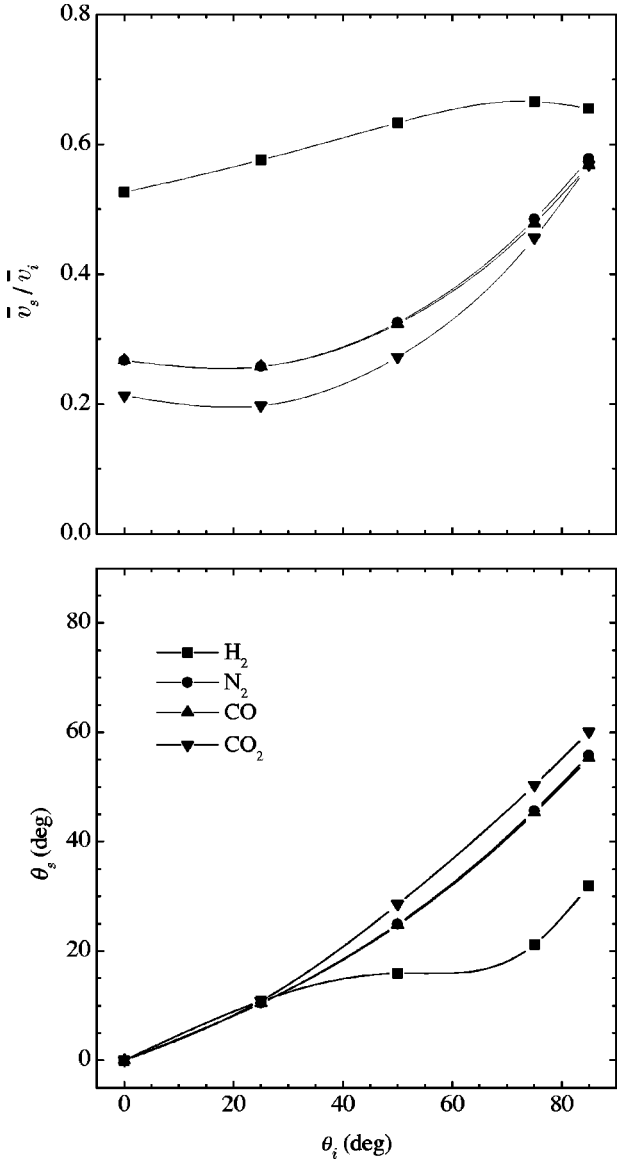

FIG. 10. The ratio $\overline{v_s}/\overline{v_i}$ and the scattering angle θ_s for H_2, N_2, CO, and CO_2 incident upon SiO_2-coated Kapton with an average velocity of 3000 m/s. These results were obtained from the measured reduced force coefficients using the interpolation method.

For a small angle of incidence, molecules with larger incident energies penetrate into the surface potential deeper than molecules with smaller incident energies. This fact would seem to indicate that molecules with larger translational energies should lose a larger percentage of their en-

ergy to the surface, become more accommodated, and scatter with smaller values of $\overline{v_s}/\overline{v_i}$ and θ_s. For large angles of incidence, the long range attractive interaction, which tends to be along the surface normal, would increase the normal momentum component while leaving the tangential component relatively unchanged, effectively decreasing the angle of incidence. The interaction time with the long range attractive potential should increase as the incident velocity decreases. Increased interaction times would increase the change in the normal momentum component. This result would imply that decreasing the incident velocity of the gas would decrease the effective angle of incidence. Thus, for a large angle of incidence, decreasing the incident velocity of the molecules would increase accommodation and the fractional energy loss to the surface, resulting in scattering with smaller values of $\overline{v_s}/\overline{v_i}$ and θ_s.

This argument could also explain why $\overline{v_s}/\overline{v_i}$ remains relatively constant, or even decreases, at large angles of incidence for H_2. The long range attractive force exerted on the incident gas by the surface would accelerate H_2 more than the other gases since it has the smallest mass, and could significantly decrease the angle of incidence H_2 has upon the surface. Thus H_2 could actually scatter with a smaller value of $\overline{v_s}/\overline{v_i}$ at large angles of incidence. As the molecules leave the surface, the decreased velocity would allow the attractive forces to act on the molecules over a longer period of time. Since this interaction will tend to be along the surface normal, the normal velocity component of the molecules will decrease more than the tangential component. As a result, the molecules would scatter with a larger value of θ_s for very large angles of incidence, but with a smaller average velocity.

To study how the scattering behavior depends upon the gas for a particular surface, independent of the average velocity of the incident molecules, the interpolation method was used to approximate the reduced force coefficients for all four gases incident upon SiO_2-coated Kapton with an average velocity of 3000 m/s. The results are shown in Fig. 10, and indicate that $\overline{v_s}/\overline{v_i}$ is largest for H_2, nearly identical for N_2 and CO, and is smallest for CO_2, while θ_s is smallest for H_2, nearly identical for N_2 and CO, and is largest for CO_2. The observation that $\overline{v_s}/\overline{v_i}$ and θ_s are nearly identical for N_2 and CO is not surprising, since the two gases have almost identical masses, they impinge upon the surfaces with nearly the same momentum, and their potential energy well depths and the anisotropies of the gas-surface interactions are most likely similar [32]. The depth of penetration into the repulsive potential energy surface will be smallest for H_2 and largest for CO_2 since H_2 has the smallest average incident energy, and CO_2 has the largest. It would then be expected that H_2 would lose the smallest percentage of its incident energy to the surface and CO_2 would lose the largest percentage. Thus H_2 would scatter with the largest value of $\overline{v_s}/\overline{v_i}$ and CO_2 would scatter with the smallest value.

Of the four gases, H_2 has the smallest, and CO_2 the largest mass. Therefore, a given force perpendicular to the direction of propagation would deflect H_2 molecules the most, N_2 and CO molecules the same, and CO_2 molecules the least, assuming the four gases propagated with same initial velocity. Thus, for large grazing angles of incidence, where the scattering is more specular, it is reasonable that the scattering angle is smallest for H_2 and largest for CO_2. For small angles of incidence, where the scattering is more diffuse, this effect is partially obscured.

In summary, it has been shown that gases scatter from the engineering type surfaces investigated in this study with a strong dependence upon the incident species and the magnitude and direction of the average incident velocity. Only for the extremely rough Z-93-coated Al surface did diffuse scattering with near complete thermal accommodation adequately describe the scattering profiles. These results demonstrate that scattering from engineering type surfaces can be nontrivial, and demonstrate much more interesting behavior than traditionally expected.

ACKNOWLEDGMENTS

This work was supported by NASA–JSC. The authors also acknowledge the technical assistance of Frank Archuleta, Jeff Patterson, and Carlos Martinez. Finally, we thank Carl Scott and Micheal Jensen at NASA–JSC for their continued support of this project.

[1] J. A. Barker and D. J. Auerbach, Surf. Sci. Rep. **4**, 1 (1985).
[2] *Dynamics of Gas-Surface Interactions*, edited by C. T. Rettner and M. N. R. Ashfold (The Royal Society of Chemistry, Cambridge, 1991).
[3] *Atomic and Molecular Beam Methods*, edited by G. Scoles (Oxford University Press, New York, 1988), Vol. 1.
[4] C. T. Rettner, J. Chem. Phys. **99**, 5481 (1993).
[5] M. L. Yu and L. A. DeLouise, Surf. Sci. Rep. **19**, 285 (1994).
[6] J. E. Hurst, L. Wharton, K. C. Janda, and D. J. Auerbach, J. Chem. Phys. **78**, 1559 (1983).
[7] S. T. Ceyer and G. A. Somorjai, in *Annual Review of Physical Chemistry*, edited by B. S. Rabinovitch, J. M. Schurr, and H. L. Strauss (Annual Reviews Inc., Palo Alto, CA, 1977), Vol. 28, pp. 477–497.
[8] M. J. Cardillo, in *Annual Review of Physical Chemistry*, edited by B. S. Rabinovitch, J. M. Schurr, and H. L. Strauss (Annual Reviews Inc., Palo Alto, CA, 1981), Vol. 32, pp. 331–357.
[9] R. Elber and R. B. Gerber, J. Chem. Phys. **79**, 4087 (1983).
[10] C. R. Arumainayagam and R. J. Madix, Prog. Surf. Sci. **38**, 1 (1991).
[11] F. O. Goodman and H. Y. Wachmann, *Dynamics of Gas-Surface Scattering* (Academic, New York, 1976).
[12] F. G. Collins and E. C. Knox, AIAA J. **32**, 765 (1994).
[13] S. M. Liu, P. K. Sharma, and E. L. Knuth, AIAA J. **17**, 1314 (1979).
[14] S. D. Rosner, R. A. Holt, and T. D. Gaily, Phys. Rev. Lett. **32**, 785 (1975).
[15] A. Yokozeki and J. S. Muenter, J. Chem. Phys. **72**, 3796 (1980).

[16] Z. Karny, R. C. Ester, and R. N. Zare, J. Chem. Phys. **69**, 5199 (1978).
[17] M. Fuchs and J. P. Toennies, J. Chem. Phys. **85**, 7062 (1986).
[18] P. R. Beuhler and R. B. Bernstein, J. Chem. Phys. **51**, 5305 (1969).
[19] P. R. Brooks, J. Chem. Phys. **50**, 5031 (1969).
[20] S. Stole, Ber. Bunsenges. Phys. Chem. **86**, 413 (1982).
[21] Z. Karny and R. N. Zare, J. Chem. Phys. **68**, 3360 (1978).
[22] C. T. Rettner and R. N. Zare, J. Chem. Phys. **77**, 2416 (1982).
[23] S. R. Cook and M. A. Hoffbauer, Phys. Rev. E **55**, R3828 (1997).
[24] E. L. Knuth, AIAA J. **18**, 602 (1980).
[25] S. R. Cook, Ph.D. thesis, The University of Texas at Austin, 1995.
[26] S. R. Cook, M. A. Hoffbauer, J. B. Cross, H. Wellenstein, and M. Fink, Rev. Sci. Instrum. **67**, 1781 (1996).
[27] J. J. Valentini, M. J. Coggiola, and Y. T. Lee, Rev. Sci. Instrum. **48**, 58 (1976).
[28] H. Pauly, in *Atomic and Molecular Beam Methods*, edited by G. Scoles (Oxford University Press, New York, 1988), Vol. 1, pp. 124–152.
[29] D. J. Auerbach, in *Atomic and Molecular Beam Methods* (Ref. [28]), pp. 362–379.
[30] D. R. Miller, in *Atomic and Molecular Beam Methods* (Ref. [28]), pp. 41–44.
[31] J. Harris, in *Dynamics of Gas-Surface Interactions*, edited by C. T. Rettner and M. N. R. Ashfold (The Royal Society of Chemistry, Cambridge, 1991), pp. 1–46.
[32] G. A. Somorjai, in *Principles of Surface Chemistry* (Prentice-Hall, Englewood Cliffs, NJ, 1972).